Author(s): Hulkko, Eero; Ahokas, Jussi; Lindgren, Johan; Myllyperkiö, Pasi; Pettersson, Mika

Title: Electronic spectroscopy of I2-Xe complexes in solid Krypton

Year: 2012

Version:

Please cite the original version:

Hulkko, E., Ahokas, J., Lindgren, J., Myllyperkiö, P., & Pettersson, M. (2012). Electronic spectroscopy of I2-Xe complexes in solid Krypton. Journal of Chemical Physics, 136(17), 174501. https://doi.org/10.1063/1.4706521

Electronic spectroscopy of I2–Xe complexes in solid Krypton

Eero Hulkko, Jussi Ahokas, Johan Lindgren, Pasi Myllyperkiö, and Mika Pettersson

Citation: The Journal of Chemical Physics **136**, 174501 (2012); doi: 10.1063/1.4706521
View online: http://dx.doi.org/10.1063/1.4706521
View Table of Contents: http://scitation.aip.org/content/aip/journal/jcp/136/17?ver=pdfcov
Published by the AIP Publishing

Electronic spectroscopy of I_2–Xe complexes in solid Krypton

Eero Hulkko,[a] Jussi Ahokas, Johan Lindgren, Pasi Myllyperkiö, and Mika Pettersson
Nanoscience Center, Department of Chemistry, University of Jyväskylä, P.O. Box 35, FIN–40014, Finland

(Received 4 November 2011; accepted 10 April 2012; published online 1 May 2012)

In the present work, we have studied ion-pair states of matrix-isolated I_2 with vacuum-UV absorption and UV-vis-NIR emission, where the matrix environment is systematically changed by mixing Kr with Xe, from pure Kr to a more polarizable Xe host. Particular emphasis is put on low doping levels of Xe that yield a binary complex I_2–Xe, as verified by coherent anti-Stokes Raman scattering (CARS) measurements. Associated with interaction of I_2 with Xe we can observe strong new absorption in vacuum-UV, redshifted 2400 cm^{-1} from the X → D transition of I_2. Observed redshift can be explained by symmetry breaking of ion-pair states within the I_2–Xe complex. Systematic Xe doping of Kr matrices shows that at low doping levels, positions of I_2 ion-pair emissions are not significantly affected by complexation with Xe, but simultaneous increase of emissions from doubly spin-excited states indicates non-radiative relaxation to valence states. At intermediate doping levels ion-pair emissions shift systematically to red due to change in the average polarizability of the environment. We have conducted spectrally resolved ultrafast pump-probe ion-pair emission studies with pure and Xe doped Kr matrices, in order to reveal the influence of Xe to I_2 dynamics in solid Kr. Strikingly, relaxed emission from the ion-pair states shows no indication of complex presence. It further indicates that the complex escapes detection due to a non-radiative relaxation. © *2012 American Institute of Physics*. [http://dx.doi.org/10.1063/1.4706521]

I. INTRODUCTION

Molecular iodine (I_2) has been a real workhorse of spectroscopic and dynamic studies in all possible phases. As a consequence, rather detailed picture of electronic state structure and spectroscopy of this diatomic model system has been developed during the past decades, especially in the gas-phase.[1,2] According to Mulliken's classification, electronic states of I_2 can be sorted by their neutral (valence states) or ionic (ion-pair states) atomic dissociation asymptotes. Iodine has 23 valence states in the Hund's *case c* coupling scheme,[3] which correlate to neutral atomic dissociation limits (^2P). Ten of the states correlate with lowest energy dissociation asymptote $I(^2P_{3/2}) + I(^2P_{3/2})$ (shortly I+I). Another set of ten states correlate with the $I(^2P_{3/2}) + I^*(^2P_{1/2})$ (I+I*) asymptote and three states with the highest limit with $I^*(^2P_{1/2}) + I^*(^2P_{1/2})$ (I*+I*). Dissociation limits are separated in energy by spin-orbit splitting of iodine ∼8000 cm^{-1} (Ref. 1). The ion-pair states of I_2 (IP) correlate with dissociation limits, where the products are ionic: I^- (^1S) or I^+ (^3P, ^1D, ^1S). There are all together 20 IP states grouped in three distinct tiers with six IP states and one *ungerade-gerade* pair.[7] In the gas-phase the first tier is located ∼40 000–41 000 cm^{-1} above the ground state with ionic limit $I^+(^3P_2) + I^-(^1S_1)$ (Ref. 8). The six states located in first tier (in energetic order) are: $D'(2_g)$, $\beta(1_g)$, $D(0_u^+)$, $E(0_g^+)$, $\gamma(1_u)$, and $\delta(2_u)$. The second tier, ∼7000 cm^{-1} above the first tier, consists likewise of six IP states: $f(0_g^+)$, $g(0_g^-)$, $F(0_u^+)$, $G(1_g)$, $h(0_u^-)$, and $H(1_u)$ (Refs. 4 and 9).

The IP states in the gas-phase or in a symmetrical solvation environment are non-polar states in a sense that the I-atoms are undistinguishable. The IP states can be described by a simple resonance structure $^+I–I^- \leftrightarrow {}^-I–I^+$ (Ref. 10). Matrix isolation of iodine in solid rare gases provides an excellent opportunity to study and test photodynamical principles in a weakly pertubating isolated environment.[11] Perturbation of the surrounding rare gas matrix can be considered fairly mild, when I_2 valence state potentials are considered, but strong for states involving IP character. The key question is how the interaction of these states, which are non-polar for isolated molecules, with the environment modifies their properties and to what extent the interaction leads to symmetry breaking and delocalization of charge to the rare gas atoms. In this regard, there are two competing effects: (i) symmetry breaking leading to dipole formation and subsequent gain in solvation energy in a polarizable host, and (ii) exchange interaction which tends to keep the system symmetric. The existing experimental data indicates symmetry breaking for the relaxed ion-pair state in Ar and Kr hosts based on strong shift of the emission with respect to the gas-phase.[5] Another indication of matrix assisted symmetry breaking is significant bond elongation of IP states in solid Ar (0.1 Å) and Kr (0.2 Å) (Ref. 12). Simulations by Yu and Coker explained these spectral observations and gave a detailed picture of the partial charge localization and strong solvation of IP states in solid argon and krypton.[10] It is however notable that no similar evidence of symmetry breaking is present in absorption of IP states, indicating that nuclear relaxation is required for this process.

The IP states have been extensively used for probing ultrafast dynamics of various valence states of I_2 through laser induced fluorescence (LIF) (Refs. 13–15). Despite the importance of these states to ultrafast dynamical studies, exact nature of these IP states seems still somewhat unclear,

[a]E-mail: eero.j.hulkko@jyu.fi.

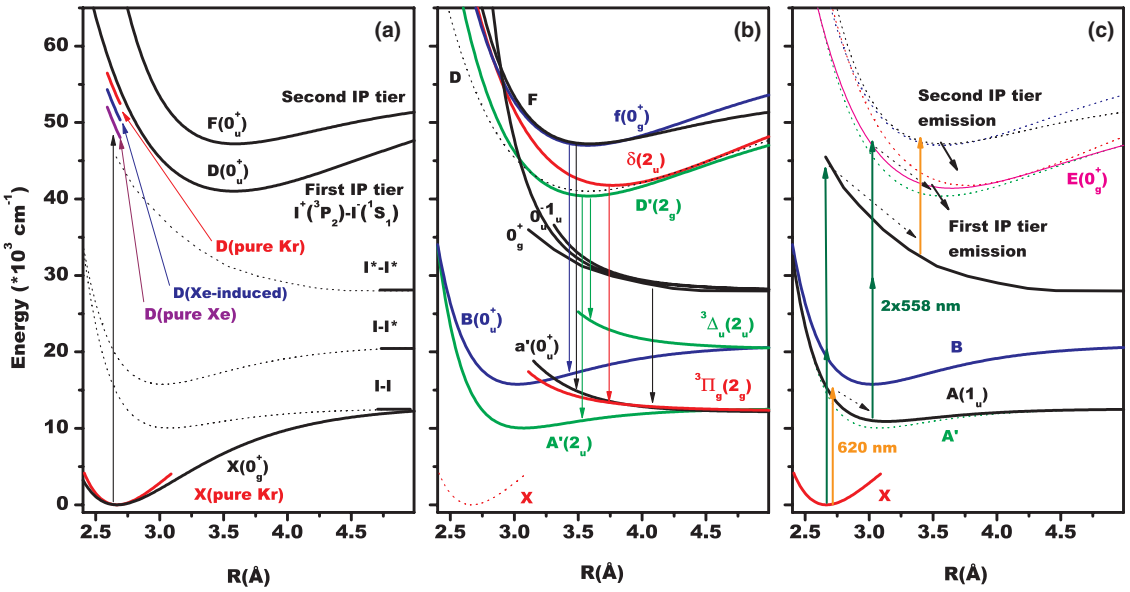

FIG. 1. Gas-phase potentials of I_2 that are relevant for this study. Panel (a) depicts the potentials that are important in VUV absorption of solid I_2/Xe/Kr ternary systems. Position of the VUV absorption in solid Kr and the effects caused by Xe are also indicated in the picture. Panel (b) shows the relevant I_2 potentials in emission. Transitions observed in this study with 193 nm excitation of mixed Kr/Xe matrices are also indicated with the colored arrows. Two possible multiphoton excitation routes and the corresponding I_2 potentials in pump-probe emission are shown in the panel (c). The shown potentials in the panel (c) relate to excitation with two femtosecond laser pulses centered at $\lambda_{Pump} = 558$ nm and $\lambda_{Probe} = 620$ nm, as will be discussed in the Sec. III C. The potentials in the Figure 1 have been constructed from multiple different sources (Refs. 1–6 and the references therein).

and has therefore attracted much recent revival of interest. In particular, relaxation and dissociation mechanisms through dense IP state manifolds and amplified spontaneous emission upon laser excitation,[16–18] influence of foreign molecules to the relaxation,[9,19] and dynamics of IP states[7,20,21] are of high current interest, especially in the I_2 gas-phase spectroscopy.

One of the major goals in the femtochemistry research is not only to measure dynamics but also to control the processes by electromagnetic fields. In this regard, condensed rare gases are particularly well suited for developing and testing control strategies involving dynamics of charge-transfer states. We have recently suggested a scheme for controlling a bimolecular reaction between iodine and a xenon atom via preparation of ground state vibrational wavepackets using coherent Raman techniques.[22] However, the realization of this scheme requires detailed knowledge of the spectroscopy of iodine and I_2–Xe complex in solid rare gases. In this work, we present VUV-absorption, UV-VIS-NIR emission, fs-CARS, and pump-probe studies of I_2/Xe/Kr ternary systems with the goal of developing a thorough picture of the nature and spectroscopy of the interaction between ion-pair states of iodine and xenon in solid rare gases. Figure 1 depicts relevant I_2 gas-phase potentials for this work with observed transitions in mixed matrices of Kr and Xe.

II. EXPERIMENTAL

Gaseous samples containing iodine and rare gas (Kr and/or Xe, AGA) were prepared in a high vacuum system, which was typically evacuated to 10^{-6} mbar pressure prior to sample preparation. Solid iodine was purified by several annealing-freezing cycles under a high vacuum condition, and iodine was stored in a Pyrex bulb connected to a sample preparation system. In order to find stable iodine pressure, iodine was left to sublimate up to vapor pressure of 0.20–0.30 Torr. When stable iodine pressure was obtained, rare gas was added until ratio of I_2/Rg$\sim$1/2600 was reached. Samples containing both Xe and Kr were prepared in the same manner as described above.

A continuous flow liquid helium cryostat (Janis Research Company, Inc.) was used to maintain low temperatures for matrix preparation and experiments. The cryostat was equipped with MgF_2 windows and a thin (150 μm) sapphire sample substrate. The cryostat was evacuated to $\sim 10^{-6}$ mbar prior to cooling. Matrix deposition onto a cold sapphire substrate was controlled with a needle valve (Leybold) and a capacitance manometer (MKS), and temperature of the substrate was measured with a silicon diode and controlled with a Lakeshore 330 temperature controller. Typical deposition rate was $\sim$0.1 mmol/min and total deposited amount was $\sim$4 mmol. Optically acceptable matrices for VUV absorption, fs-CARS, and pump-probe measurements were obtained at 40 K for krypton and mixed matrices, and at 50 K for pure xenon matrix. In emission experiments, 19 K and 40 K were chosen as deposition temperatures for krypton and xenon, respectively. Emission spectrum of I_2 in solid Kr showed similar spectral features after deposition at 40 K and 19 K. All measurements were carried out at 5–50 K.

Detection system used in absorption and emission measurements was constructed from an image intensified charge coupled device (ICCD, Andor) and a 12.5 cm spectrograph (Oriel MS 125) equipped with 600 (blaze wavelength 200 nm), and 400 (blaze wavelength 500 nm) grooves/mm gratings. In absorption measurements, a D_2 lamp (Cathodeon) was used as a VUV/UV light source. In VUV measurements,

oxygen was removed from the light path outside the cryostat by an efficient nitrogen purge. Laser induced fluorescence was recorded upon excitation of sample at 193 nm by an ArF excimer laser (Optex, pulse length 5–10 ns). Methanol in a 1 cm quartz cuvette was used to reduce laser line at 193 nm before the detection system and an optical cut-off filter was used to filter out 2nd order diffraction emission lines. Lifetime measurements were carried out by a time gated ICCD, where time gating and delays were set up with a delay generator (Stanford Research Systems). The term "delay" in emission refers to the time when the measurement gate opens after a triggering pulse to the excitation laser. The delay parameter was experimentally adjusted to a value t = 770 ns. At this time position first rising emission component was observed in the spectra of I_2 samples after the laser excitation. Note that the absolute value of the delay t has *no* physical significance. It only approximately defines the starting position of emission in our experimental setup. This fixed t value was used in most emission experiments. In some experiments the delay value was adjusted 200 ns further in time (t+200 ns) in order to filter out fast emission components. The term "gate" defines gathering time of emission after the set delay (typically for short gating 20 ns or for long gating 6 μs or 10 μs).

Femtosecond CARS (fs-CARS) and pump-probe measurements were carried out using three non-collinear optical parametric amplifiers (NOPAs) generating the used Pump, Stokes (used only in fs-CARS measurements), and Probe pulses. Our home-built NOPAs were pumped by a second harmonic radiation (400 nm) of an integrated femtosecond Ti: sapphire laser (Coherent Libra), with a ~1 mJ output at 800 nm with a repetition rate of 1 kHz. Alternatively, a commercial OPA (TOPAS, Light Conversion Ltd.), pumped with a fundamental frequency of the femtosecond laser, was used for generation of probe pulse in some experiments. Pulses were delayed using a computer controlled delay line (Aerotech) with a step of 20 fs. Temporal widths of the pump, Stokes, and probe pulses were approximated by autocorrelation measurements to be ~50–60 fs when NOPAs were used, and ~100 fs (uncompressed) when commercial OPA was used. A cooled photomultiplier tube (PMT) was used for detection of spatially and spectrally filtered coherent CARS signal. Incoherent spectrally resolved pump-probe signal was detected as a function of probe delay using the time gated ICCD described above, with the exception that no spectral filtering of the signal was used. The pump-probe setup was also used to study "non-dynamical" dissociation of I_2 in solid Xe at T = 10 K and T = 50 K. The I_2/Xe samples were irradiated with 548 nm fs-pulses, while simultaneously measuring the changes in incoherent emission generated by the fs-pulses as a function of irradiation time.

III. RESULTS

A. UV/VUV absorption

Figure 2 shows VUV/UV absorption spectra of I_2, in pure Kr (Xe = 0%), in slightly Xe doped Kr matrices, with varying Xe/Kr ratio (Xe = n%), and in pure Xe matrix (Xe = 100%) at 40 K. The absorption spectra have been baseline corrected

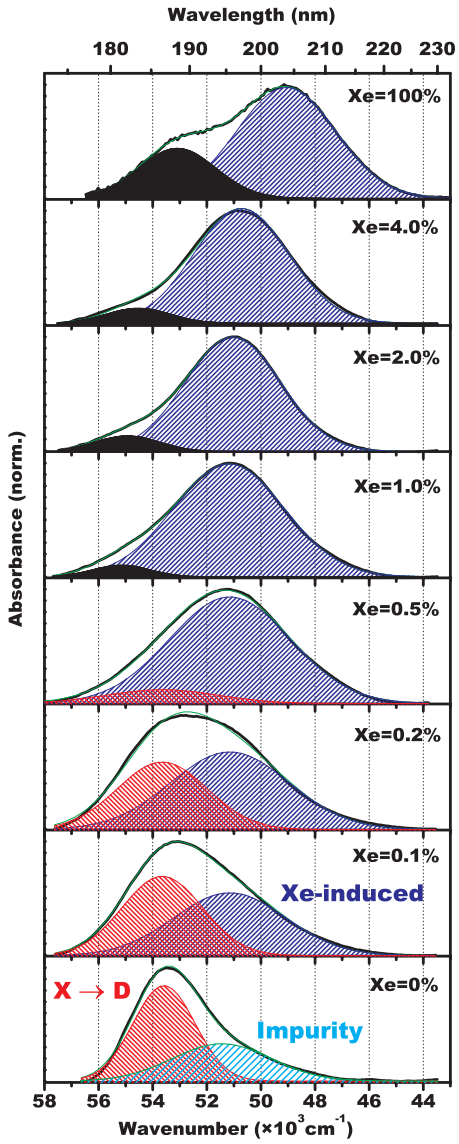

FIG. 2. VUV/UV absorption spectra of I_2 in pure krypton (Xe = 0%), in xenon doped krypton (Xe = 0.1–4.0%), and in pure xenon (Xe = 100%). All the spectra have been recorded at 40 K and normalized to respective absorption maxima. Spectrum labels denote xenon pressure percentage in the gaseous host matrix (Xe = p(Xe)/(p(Kr) + p(Xe)) * 100%). I_2/Rg (Rg = Kr + Xe) ratio was ~1/2600 in all experiments. For explanation of different patterns in the picture, see text.

with a suitable linear function in the shown region and normalized to the maxima of the absorption feature. In the pure Kr case (Xe = 0%), the absorption contains a strong main feature ($\tilde{\nu}_{max}$ = 53 600 cm^{-1}), and a broad shoulder-like feature to the red from the main band ($\tilde{\nu}_{max}$ = 51 400 cm^{-1}). Two absorptions are qualitatively shown by a fit with two Gaussian functions in the lowest spectrum in Figure 2. The area of the main feature is highlighted with a dense red diagonal pattern, and the shoulder feature with a cyan pattern. The main feature in pure krypton has been reported previously and assigned as X → D (ground state to D ion-pair state) electronic transition,[5] and has been assigned as such in the Figure 2. The intensity of the red wing showed slight variation between samples and it could be bleached under static D_2-lamp irradiation, with very long time scales. Also, intensity of the

transition decreased upon purification of iodine, implying that the feature probably belongs to an impurity in I_2.

Significant change in absorption spectrum can be observed when Xe is added to the sample. The apparent shape of the absorption broadens, and the maximum of the whole VUV absorption feature shifts strongly toward lower energies, even with trace amounts of Xe. Even though absorptions are not spectrally well resolved, the change can easily be explained by appearance of a new redshifted absorption, induced, and enhanced by the increasing presence of Xe in the I_2/Kr matrix ($\tilde{\nu}_{max} = 51\,200$ cm^{-1}, redshift of 2400 cm^{-1}). Varying the Xe doping ratio from 0% to 0.5% (four lowest spectra in Figure 2), reveals a systematic increase in the relative intensity of the redshifted absorption. In an attempt to capture the shape change and the redshift with low Xe doping, the VUV absorption feature has been fitted with two Gaussian functions, representing the main absorption present in the I_2/Kr (red pattern) and the Xe-induced band in the mixed matrices (blue pattern). Note that the enhanced absorbance is located almost exactly on top of the presumed impurity absorption already present in pure Kr. Nonetheless, already at the doping level of 0.1%, the increase of the intensity induced by interaction of iodine with Xe is clearly distinguishable.

It is remarkable that the intensity of the 51 200 cm^{-1} band is comparable with the intensity of the I_2 band at 53 600 cm^{-1}, even with a Xe ratio of 0.1%. With Xe ratio of 0.5% the Xe-induced band already completely dominates the absorption spectrum. We also observe some bleaching of the Xe-induced band with D_2 irradiation, but our results are inconclusive in this regard. While doping with low levels of Xe causes a dramatic shape change, and strong redshift of the absorption band, the more extensive doping gradually redshifts Xe-induced absorption toward the absorption band maximum of I_2 in pure Xe matrix. More extensive doping reveals yet another spectral feature, not observed in the pure Kr, and in the lowest Xe doping levels. Blue wing of the absorption feature appeared and gained intensity upon more extensive Xe doping. Appearance of this new feature ~55 200 cm^{-1} (highlighted with a black interior) is also included in our fitting procedure. New absorption is already weakly visible at Xe = 1.0%, and more clearly at higher Xe ratios. Going from low xenon levels toward pure xenon, the Xe-induced band (51 200 cm^{-1}), and the blueshifted band (55 200 cm^{-1}) both show very distinctive redshift of 2100 cm^{-1} to 49 100 cm^{-1}, and to 53 100 cm^{-1}, respectively.

B. Emission

The effect of Xe doping in emission after 193 nm excitation is represented in Figure 3. In krypton (Xe = 0%) main emission was observed in ~26 000–23 000 cm^{-1} region, and less intensive emission doublet in the visible region with maxima at 17 300 cm^{-1} and 15 900 cm^{-1}. The main emission band structure at ~26 000–23 000 cm^{-1} has an intense central peak at 24 000 cm^{-1} and distinctive shoulder at 24 900 cm^{-1}, more clearly resolved at T = 5 K (not shown). Observed emissions in krypton have been previously characterized as transitions originating from the two lowest ion-pair

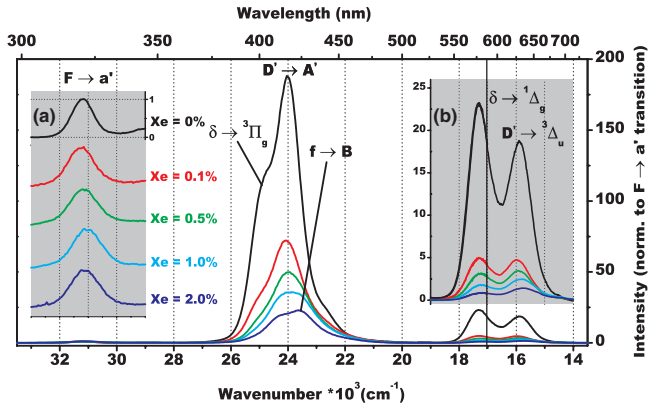

FIG. 3. Emission spectra of I_2 obtained after 193 nm excitation in pure krypton (Xe = 0%, black spectrum), and in slightly Xe doped krypton (Xe = 0.1%–2%, color coded spectra) matrices at 19 K. All spectra are normalized to UV transition shown in the grey inset (a), where the tentatively assigned F → a′ transition is slightly offsetted for clarity. Thus, the spectra in the main picture and inset (b), represent changes of emission relative to the F → a′ transition. Tentative assignments of other ion-pair emissions are indicated in the picture. Note that the spectra are composition of two different measurements, one in the UV-region with a very short time gate (gate width 20 ns), and one in the visible region with a long time gate (gate width 6 μs). Different measurements are separated in the picture with black vertical line. A fixed time delay of t was used in all measurements. In the pure krypton case both regions have been measured with a same gate width of 10 μs. The spectra are uncorrected for spectral response of the detection system.

tiers to various valence states of I_2, and have been tentatively assigned[5,10,23,24] in the Figure 3. Exciting the I_2/Kr matrix with ArF laser results also in a weak emission in the UV-region at 31 200 cm^{-1}, now assigned as F → a′ transition.[25]

Most pronounced change in emission as function of Xe doping (between 0.1% and 2%) is a systematic loss of intensity from the main emission structure and the visible region emissions relative to the UV-emission. The intensity loss effect is very dramatic even with our lowest Xe ratio of 0.1%, and continues systematically to higher Xe ratios. Slightly less pronounced effects of Xe doping are the spectral changes in the UV-emission (31 200 cm^{-1}), the main emission (26 000–23 000 cm^{-1}), and the visible emissions (17 300 cm^{-1} and 15 900 cm^{-1}). The UV-emission shows a mild redshift of ~100 cm^{-1}, going from Xe = 0% to Xe = 2%. However, we note that our experimental accuracy is of the same order (100 cm^{-1}). Second, blue shoulder of the main emission with maximum at 24 900 cm^{-1} is reduced relative to the most intense band in the main structure at 24 000 cm^{-1} with increasing amount of Xe in the matrix. Simultaneously, the red-wing of the main feature is enhanced and begins to resemble a peak-like structure with a maximum at 23 600 cm^{-1}, most clearly visible in the spectrum with 2% of Xe. In order to highlight the observed change in the main emission, difference spectra of Xe doped matrices compared to pure Kr case is represented in Figure 4, where spectra have been normalized to the center (24 000 cm^{-1}) of the main emission. Associated with the relative change in the main feature, emissions in the visible region (15 900 cm^{-1} and 17 300 cm^{-1}) exchange their relative intensities in favor of the red-most feature. The red-most emission in the visible region shows an apparent redshift of ~200 cm^{-1} while the position of the blue-most emission is

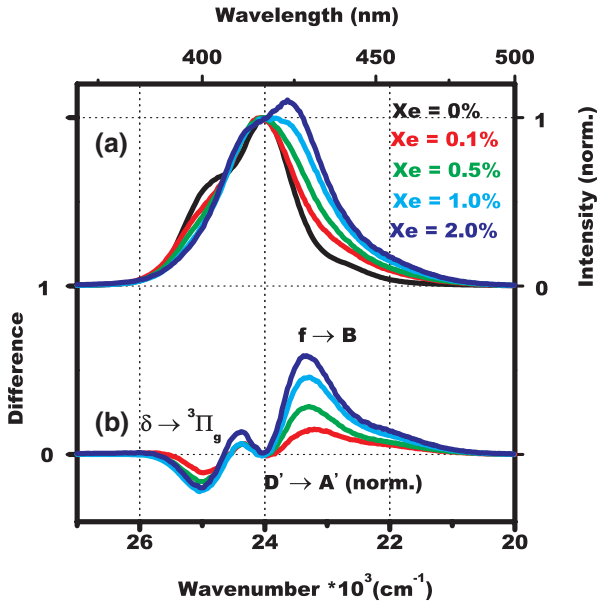

FIG. 4. Spectral changes of I_2 main emission upon Xe doping of Kr matrix at 19 K. Panel (a) shows the normalization to center of emission at 24 000 cm^{-1}. Panel (b) shows the difference between normalized Xe doped emissions vs. emission in pure krypton. Color coding in the panel (b) relates to the Xe doping ratio in the panel (a). In the bottom panel the spectrum with certain color is the top panel spectrum with the same color minus the spectrum in pure Kr (black spectrum in panel (a)). The shown spectra are the same as shown in Figure 3 with short time gating and different normalization.

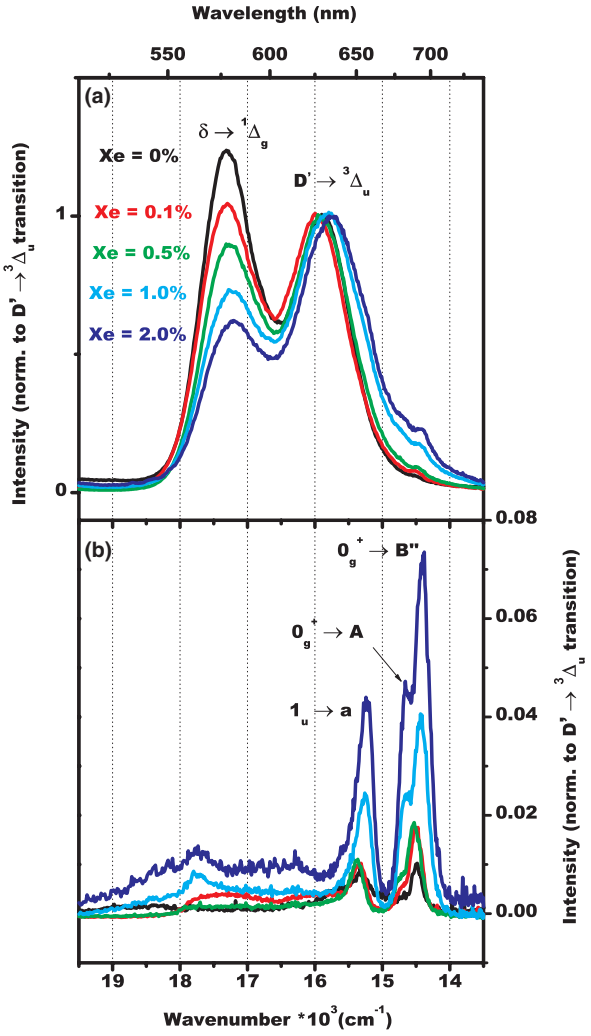

FIG. 5. Spectral changes of I_2 emission in the visible doublet region upon Xe doping of Kr matrix at 19 K. Panel (a) shows the emissions normalized at 15 900 cm^{-1} with gate delay of t. Panel (b) shows the same spectra with a larger time gate delay of t + 200 ns. Normalization constant used in the panel (a) has been used in the panel (b). The spectra have been measured with same gate widths as the visible region in Figure 3 (10 μs for I_2/Kr and 6 μs for the Xe doped).

effectively unaffected by the Xe presence within this range of Xe ratios. Exchange of relative intensity ratios in the visible region is clearly shown in the top-most panel (a) of Figure 5, where the emissions are normalized to the red-most emission of the visible doublet.

All of the emissions shown in Figure 3 have very short lifetimes, of the order of 20 ns in pure Kr and slightly Xe doped matrices. However, Xe doping induces another spectral change already weakly visible in the panel (a) of the Figure 5. Increasing Xe in the matrix enhances long lived (lifetime of ~4 μs) and sharp visible transitions at 14 400 cm^{-1}, 14 800 cm^{-1}, and 15 400 cm^{-1}, relative to the red-most emission at 15 900 cm^{-1}. Observed long lived transition have also been characterized as emissions originating from doubly spin-excited (I*+I*) repulsive valence states of I_2, which are stabilized by the surrounding matrix cage.[26] In order to clarify the positions and relative intensity change of the long lived transitions, delay of the time gate was adjusted from t to t + 200 ns. This procedure effectively filters out the fast emissions shown in the panel (a) of the Figure 5, leaving only the very long lived emissions shown in the panel (b). Normalization factor used in panel (a) was also imposed on the spectra in panel (b). Significant changes in emission can be observed when large amount of Xe is added to the matrix (2%–50%), or Kr environment is completely changed to Xe. Figure 6 represents how observed emissions change from pure Kr to pure Xe. Shape of the main emission at ~26 000–23 000 is narrowed, and redshifted by 700 cm^{-1} (from maxima in Kr at 24 000 cm^{-1}), in a range of Xe = 0% to 17%. In the same range of Xe ratios the UV-emission shows a similar redshift of 500 cm^{-1}. Simultaneously, the visible doublet of ion-pair emissions disappears almost completely, and are replaced by spin-orbit transitions shown in the Figure 5. The long lived spin-orbit transitions show only a mild redshift ~100 cm^{-1} within range of Xe = 0%–17%. With the Xe ratio of 50%, emission spectrum looks dramatically different from spectra from samples with less Xe. Even though the main emission observed at lower Xe ratios is possibly still weakly present (redshifted to ~23 000 cm^{-1}), the spectrum is dominated by a new broad emission with a maximum at 25 800 cm^{-1}. It is also clear that sharp spin-orbit transitions in the visible region have gained strength. Going from 50% to pure Xe matrix, the spin-orbit transitions continue to increase their relative intensity, and the broad emission in the 25 800 cm^{-1} changes its shape to a continuum-type of emission with a distinct maximum at 26 500 cm^{-1}. Associated with the increase in the continuum-type of emission, weaker emissions around 19 000 cm^{-1} and 22 000 cm^{-1} gain also strength, implying common origin of the emissions. These transitions have

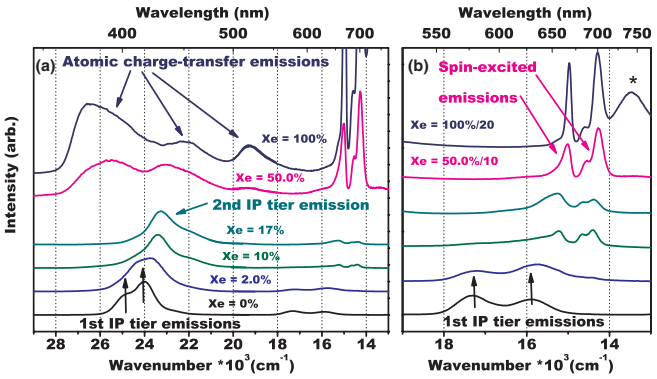

FIG. 6. Emission spectra of I_2 with 193 nm excitation from pure krypton (Xe = 0%), to pure Xe, at 19 K. Panel (a) shows the measured spectra from UV-region to visible region. The shown spectra are again composition of two measurements, but in this case the both regions have been measured with long time gate width of 10 μs, except for the Xe = 2.0%, where the parameters used were 200 ns for the UV-region, and 6 μs for the visible region. Spectra have been normalized to the maxima of the main emission in the 26 000–23 000 cm^{-1} region and offsetted for clarity. Panel (b) is an enlargement of the visible region. Presumed origin of the different transitions is indicated in the picture. The spectrum Xe = 100% contains presumably an artifact emission marked with an asterisk. The shape and the energy implies that emission is a second order diffraction of the continuum-type of emission with a maximum at 26 500 cm^{-1}.

longer life-times (~130 ns) than the IP emissions observed in the pure Kr.

We performed I_2 dissociation studies in solid Xe at T = 10 K and T = 50 K by irradiating the sample with fs-548 nm excitation (corresponding to two-photon excitation of ~274 nm). In these studies we could only observe increase of the broad 25 800 cm^{-1} emission and the increase of two visible emissions (19 000 cm^{-1} and 22 000 cm^{-1}). Simultaneously sharp spin-orbit transitions decreased their intensity. No evidence of other transitions were observed in the irradiation studies (see supplementary material S1 for details[29]).

C. Fs-CARS and pump-probe

Two matrices with different Xe doping levels were selected for femtosecond pump-probe studies: I_2/Kr matrices with Xe = 0% and Xe = 0.1%. Before pump-probe measurements were carried out, the samples were characterized by using fs-CARS technique. In the case of Xe = 0%, the fs-CARS signal showed expectedly only presence of isolated I_2 (Refs. 6 and 27). When the matrix sample was doped with Xe = 0.1%, in addition to signal from I_2 we could observe definite signal from isolated 1:1 I_2–Xe complex.[22,28] The fs-CARS characterization of the matrix with Xe = 0.1% essentially reproduced the our earlier results for high vibrational wavepacket[22] showing that the matrix with Xe = 0.1% already contains significant amount of I_2–Xe complex (see supplementary material S2 for details of the fs-CARS measurements[29]).

Spectrally and temporally resolved pump-probe emissions from the matrix with Xe = 0.1%, upon excitation with two femtosecond laser pulses (λ_{Pump} = 558 nm and λ_{Probe} = 620 nm) are shown in the top panel of Figure 7. The contour image represents time-resolved relaxed emission as a function of delay between the pulses. Analogous measurement was performed for I_2/Kr matrix as well (not shown). With negative time delays (Probe arriving to the sample before Pump) emission in the 420 nm region is many times stronger than on the positive side (Pump before Probe). There is a clear change of emission as the pulse delay changes from negative to positive. The spectral change is shown in the panels (a) and (b) of the Figure 7. The panel (a) shows spectra at negative time delay of −3 ps for samples with Xe = 0% and Xe = 0.1%. The lower panel (b) shows corresponding data at positive time delay of +3 ps. Individual transitions have also been suggested in the spectral cuts, where the red and green transitions at t = −3 ps correspond to the first IP tier transitions (D′ → A′, $\delta \rightarrow {}^3\Pi_g$), and the blue transitions at t = +3 ps to the second IP tier transitions (F → a′, f → B), observed also with a direct 193 nm excitation (see Figure 3). Time evolution of the D′ → A′ emission (green in panel (a)) is shown in the panel (c) for matrices with Xe = 0% and Xe = 0.1% on the negative delay side. The same for the f → B emission (blue in panel (b)) on the positive side is shown in panel (d). Fitted areas of the respective transitions are depicted in the panels (c) and (d). The matrix with Xe = 0.1% was also studied with different pulse energies (λ_{Pump} = 558 nm and λ_{Probe} = 500 nm, see supplementary material S3 for details[29]). This combination probes the B-state dynamics in a 1 + 1 photon process.[15] Clear oscillations of the wavepacket on the B-state are evident in all of observed emission bands (period of 360 fs), similarly in pure Kr and Xe doped matrix.

IV. DISCUSSION

A. Absorption

In undoped Kr (Xe = 0%), the strong feature at 53 600 cm^{-1} is with great certainty due to the electronic transition from the I_2 ground state $X(^1\Sigma_g^+,0_g^+)$ to the $D(0_u^+)$ IP state, based on the dominant $\Delta\Omega = 0$ selection rule governing the electronic transitions in the *Hund's case c* type coupling (see Figure 1(a)). The transition is slightly redshifted from the gas-phase[30] ($\Delta\tilde{\nu}_{gas-Kr}$ = 1200 cm^{-1}), due to the dielectric solvation of the surrounding matrix. By a simple notion that we could observe a slight increase in the intensity of the broad redshifted band at 51 400 cm^{-1} within time scale of weeks when I_2 was stored in our vacuum system, with the observation that the band intensity decreased upon purification of I_2, implies strongly toward "impurity" origin of the band. Our VUV absorptions are in a good agreement with the previous results by Helbing and Chergui.[5] In our measurements the X → D transition has a maximum at 53 600 cm^{-1} with FWHM of 2700 cm^{-1} and a bleaching broad-red wing at 51 400 cm^{-1}, with FWHM of 4300 cm^{-1}. In Ref. 5, the maxima (and the widths) were at 53 600 cm^{-1} (~3100 cm^{-1}) and 51 500 cm^{-1} (3900 cm^{-1}), respectively. Alternative explanation for the observed VUV transitions has also been suggested by Bihary *et al.*, based on different bleaching rates of the absorptions upon 193 nm excitation and the gas-phase energetics of the IP states.[25] They tentatively argued that the red-wing (now assigned as impurity) is actually the parallel X → D and the main emission is the perpendicular X → $\gamma(1_u)$ separated in

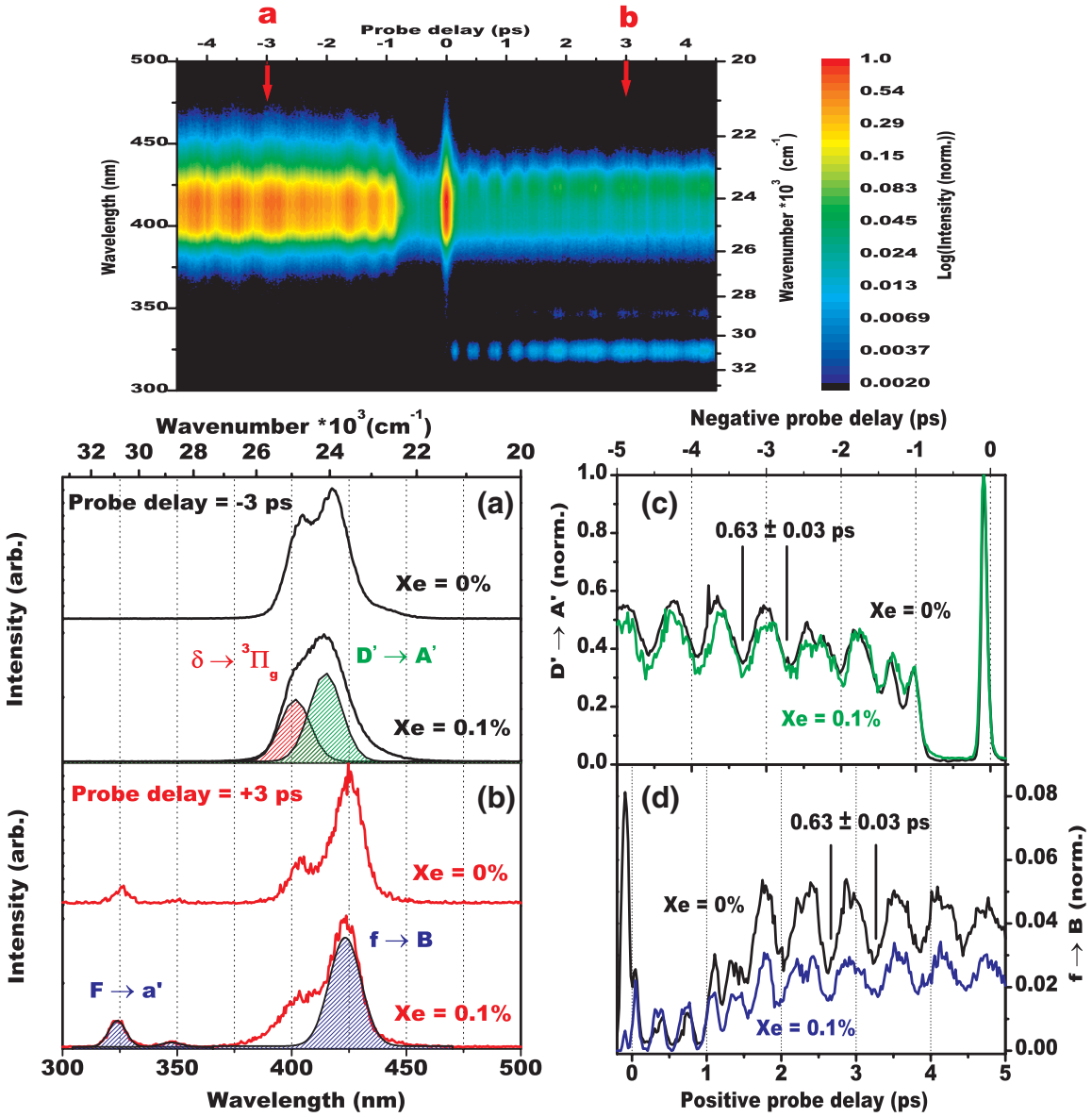

FIG. 7. Top panel is a pump-probe emission contour of I_2/Kr matrix with 0.1% of Xe at T = 10 K, where $\lambda_{Pump} = 558$ nm and $\lambda_{Probe} = 620$ nm. Contour has been measured with fast gating (60 ns). Intensity (z-axis) is normalized to the maximum of the main emission at t = 0 ps. Normalized intensity is shown in logarithmic scale to highlight weak emissions in the positive time delays. Lower panels (a) and (b) show spectral cuts measured at probe delays = ±3 ps for matrix without Xe and with 0.1% of Xe. Individual transitions have been highlighted in the spectra of Xe = 0.1%. Lower panels (c) and (d) shows the time evolutions of fitted areas of D′ → A′ and f′ → B emissions for matrices with Xe = 0% and Xe = 0.1%.

the gas-phase by ~600 cm^{-1}. The generated dichroism when unpolarized light is used is responsible for the lack of intensity in X → D. Even though we cannot completely refute this argument, because of we have not measured our VUV spectra with polarized optics, their argument seems very unlikely in the light our observation of the increasing intensity in the redshifted band as a function of storage time.

When Xe is added to Kr matrices, strong systematic change is observed in the VUV absorption (see Figure 2). Importantly, a new feature at 51 200 cm^{-1} (redshift of 2400 cm^{-1}) appears already at 0.1% doping level. Kiviniemi *et al.* have previously characterized in great detail the effect of Xe on the I_2 ground state vibrational frequency in Kr matrices using the fs-CARS technique.[28] In this earlier publication by our group it was estimated from the band amplitudes of I_2 and I_2–Xe complex that a ratio as high as ~1/3 of the I_2 molecules are in the 1:1 complex form, when Xe to Kr ratio is 0.1% and I_2/Kr = 1/2600. Our CARS results, where we have prepared our matrices with identical gas ratios and matrix preparation parameters (temperature, flow rate) are in a good qualitative agreement with the earlier results, implying that in our case at least significant part of the iodine molecules are in the 1:1 complex form (see supplementary material S2 for details[29]). The CARS observations indicate directly that the new absorption feature in the slightly Xe doped matrices most likely belongs to the *1:1 I_2–Xe complex* isolated in solid Kr environment.

Even though VUV absorptions of molecular I_2 are fairly well understood in the gas-phase (see Ref. 1), very limited number of studies actually concern environmentally mediated

changes of absorption of these high energy IP states, or effects induced by the solid environments. To our knowledge VUV absorption in solid Xe has not been reported previously. On the other hand, it is well-known that iodine forms complexes with many hydrocarbons that show clear charge-transfer absorptions which are strongly redshifted from the IP absorption of iodine, classic example being the I_2-benzene complex[31–34] with a strong charge-transfer absorption slightly below 300 nm. In the present case the Xe induced absorption in the VUV is broadened from 2700 cm^{-1} to 4800 cm^{-1} implying that the excited state has changed character. It is not however obvious, what is the exact nature of the Xe-induced absorption. Two plausible explanations can be suggested in the case of isolated I_2–Xe complex:

- the state is a charge-transfer state between complex partners (Xe^+–$(I_2)^-$).
- the state is a "pure" IP state of iodine (I^+–I^-), which is symmetry broken by the Xe atom in the first solvation shell, resulting in a permanent dipole state.

To elaborate the *first* possibility, we can make an estimation where the charge-transfer absorption would be in the matrix isolated I_2–Xe complex using

$$E(I_2^- - Xe^+) = IP(Xe) - Ea(I_2) + C, \tag{1}$$

where IP(Xe) is the first ionization potential of Xe (IP(Xe) = 12.12 eV (Ref. 35)), and Ea(I_2) is the vertical electron affinity of I_2 (Ea(I_2) = 1.7 eV (Ref. 36)). The term C is the Coulombic potential between charges. In our estimation, for the two plausible complex geometries (linear and T-shaped), a negative charge (on I_2 molecule) is localized evenly between point-like I atoms (each carries −1/2e charge) and Xe acts as a positive point charge. The C-term has been calculated using known ground state I-I distance of 2.666 Å and MD-simulated Xe–I_2-distances (Xe to center of I_2 mass) of 6.01 Å in the linear complex, and 3.47 Å in the T-shaped complex.[28] This simple calculation gives estimation of 7.9 eV (63 700 cm^{-1}) for absorption maximum of the linear complex and 6.6 eV (52 800 cm^{-1}) for the T-shaped complex. The electrostatic solvation inside Kr matrix can be estimated using classical solvation models introduced by Onsager[37]

$$\Delta E = \frac{1}{4\pi\epsilon_0}\frac{8(\epsilon-1)(\Delta\mu)^2}{(2\epsilon+1)d^3}, \tag{2}$$

where ϵ is the dielectric constant of Kr (ϵ = 1.784 (Ref. 38)), $\Delta\mu$ is the difference of dipole moments between the ground state ($\mu_G = 0$) and the charge-transfer state ($\mu_{CT,\,linear}$ = 28.9 D, $\mu_{CT,\,T-shape}$ = 17.9 D), and the d is the diameter of a spherical cavity (d = 8.43 Å (Ref. 39)). We can expect the charge-transfer band of I_2–Xe to be further redshifted in the linear complex ∼1.1 eV and in the T-shaped complex ∼0.4 eV. The charge-transfer absorption (I_2^-–Xe^+) can be expected to be very close in energy (estimated 54 400 cm^{-1} for linear and 49 300 cm^{-1} for T-shaped) of the first IP state tier of I_2 in solid Kr.

The *second* possible explanation for the redshifted VUV absorption is the symmetry breaking of the I_2 IP state. Helbing and Chergui concluded in their study that I_2 shows no charge delocalization to a pure solid Ne, Ar, or Kr in low temperature matrices.[5] Their VUV absorption results also imply that *absorbing* IP states of I_2 have a gas-phase-type symmetry. Manifestation of this is the abnormally small matrix shift of X → D absorption compared to the observed emissions from the first IP tier. For example, when I_2 is imbedded in a Kr matrix X → D absorption redshifts only by a 1200 cm^{-1}, while the observed emissions redshift close to a 5000 cm^{-1} from the gas-phase. Within the classical solvation model (Eq. (2)), the small matrix shift in absorption implies that no significant dipole is present within the absorbing I_2 molecule. The observed redshift of 1200 cm^{-1} from the gas-phase can be purely attributed to changes in orbital energies due to interaction with the dielectric environment. Another implication of the gas-phase-type symmetry in Ref. 5 is the fact that the line width of X → D absorption (∼3000 cm^{-1}) is very similar in the matrices and in the gas-phase. The symmetry breaking of the I_2 IP states has recently been suggested as the reason for the discrepancy between the matrix shifts in absorption and emission.[10] Yu and Coker showed using the DIM-DIIS calculations that *emitting* IP states of I_2 in solid Ar and Kr have a permanent dipole. Iodine atoms acquire partial charges (and are hence strongly solvated) when the polarizable matrix environment distorts around I_2 molecule excited to the IP state.

We think that a similar effect could explain the redshifted VUV absorption observed in the presence of I_2–Xe complex. When the iodine in the Xe-complex is excited to the D-state, close interaction with the Xe atom can, and most likely will, break the symmetry of the D-state. This causes an asymmetric charge separation between iodine atoms directly with the excitation (i.e., partially charged I atoms). This complex "D-state" has a permanent dipole that is strongly and instantaneously solvated by the Kr surroundings without the need of nuclear relaxation. It is also not unthinkable that redshifted absorption in pure Kr at 51 400 cm^{-1} has the same origin as the Xe-induced absorption, even though we cannot explicitly say what is the "impurity" in our sample. Presence of another molecule in the first solvation shell of I_2 could in principle cause identical asymmetric charge separation effect as our deliberate complexation with Xe. We also note that Xe is the most abundant impurity in our Kr gas (5.0 ppm according to the manufacturer), which could partly explain why we see such an "impurity" band already in pure Kr. Note however that distinction between the two possible mechanisms (charge-transfer, symmetry breaking), without even thinking about the combination of the mechanisms, is not reliably possible simply based on the VUV-data. Unfortunately, no comparable VUV absorption data exist for other mixed rare gas matrices that could directly implicate symmetry breaking. DIM-DIIS or gas-phase *ab initio* calculation of I_2–Xe complex IP states could possibly clarify this issue.

At higher Xe doping levels the new absorption shifts gradually to red and this can be understood by increasing the number of Xe atoms in the solvation layer. Finally, in pure xenon the band reaches its final position at 49 100 cm^{-1} implying a shift of 2100 cm^{-1} upon changing the environment from krypton to xenon. The shift of this magnitude can only be expected for a *strongly polar state*. In comparison changing matrix environment from Ne to Kr yields to shift of

600 cm^{-1} in absorption.[5] The new blue-shifted band at higher energies (55 200 cm^{-1}) undergoes a similar shift giving a good reason to believe that it belongs to a charge transfer state as well, possibly a higher energy state of the I_2–Xe complex. Plausible explanation for band would be transition to symmetry broken $F(0_u^+)$ state, which belongs to the second tier of I_2 ion-pair states. This argument can be rationalized with same strong selection rules as in the case of X → D transition ($\Delta\Omega = 0$, u ↔ g, + ↔ +). In the gas-phase X → F can be reached by single photon excitation with sychrotron radiation at 169 nm,[40] whereas the strong X → D "Cordes band system" is observed in the 170–200 nm region. Separation of the two observed transitions in pure Xe by ~4000 cm^{-1} suggest that the blue-shifted transition could indeed be the solvated X → F transition. However, assignment of this transition must be considered tentative until further proof becomes available.

In summary, upon doping a I_2/krypton matrix with Xe, two distinct processes are observed: (i) single Xe atom induced absorption, caused by the symmetry breaking of the I_2 D-state in the I_2–Xe (or possibly full or partial charge-transfer within the complex), and (ii) increasing energetic solvation of the Xe-induced state upon adding further Xe atoms, leading ultimately to a strongly polar absorbing state in solid Xe.

B. Emission

In contrast to absorption, as already stated, in emission I_2 shows strong symmetry breaking effects in solid Kr already without any doping with Xe. Emissions from the first IP tier are redshifted by 4700 cm^{-1} from the gas-phase. The broad main emission structure in solid Kr at 24 000 cm^{-1} has been assigned to multiple distinct overlapping transitions mainly from the first IP tier (see Figure 1(b)), namely $D'(2_g)$ → $A'(2_u)$ (I+I), and $\delta(2_u)$ → $^3\Pi_g(2_g)$ (I+I) (Refs. 5 and 10). The band at 24 900 cm^{-1} in solid Kr might also be $\beta(1_g)$ → $A(1_u)$ (Refs. 14 and 24). Helbing and Chergui argued based on their identical temperature behavior that 15 800 cm^{-1} and 17 100 cm^{-1} bands have common emitting states with the two bands in the main emission structure, but transitions terminate to the states with a I+I* limit. The 15 800 cm^{-1} was assigned in their work as $D' \rightarrow {}^3\Delta_u(2_u)$ and 17 100 cm^{-1} band as $\delta \rightarrow {}^1\Delta_g(2_g)$. The weak UV emission observed in this work (used for normalization in the Figure 3) has not been reported in the literature in Kr, but in analogy to solid Ar this transition can be fairly uniquely assigned to $F(0_u^+) \rightarrow a'(0_g^+)$ (I+I) (Ref. 25). This transition originates from the second IP tier, in contrast to most of the other transitions in the pure Kr case, which originate from the first IP tier. In addition to the well separated F → a′ transition, the main emission structure at 26 000–23 000 cm^{-1} presumably contains a contribution from another second IP tier transition ($f(0_g^+) \rightarrow B(0_u^+)$) with a maximum at 423 nm (23 600 cm^{-1}). This transition has been previously reported by Gühr *et al.* in solid Kr.[24] How the second IP tier transitions in solid rare gases are populated upon 193 nm excitation is unclear at the present. Plausible reason would be that excitation with 193 nm leads to a weak absorption of the F-state and the subsequent relaxed emission from the second IP tier states. However, possibility of a population from the D-state by non-abiabatic energy transfer through some unknown mechanism cannot be ruled out.

Subtle changes are observed in the emission spectrum of I_2/Kr matrices doped with small amounts of Xe (<2%). Notably, Xe doping did not induce any new emission bands or significant shifts in the existing bands. However, remarkable intensity changes in the emission bands take place in this doping range. In particular there is clear tendency that the relative intensities of the emissions from the second IP tier states increases at the expense of the first tier IP states (see Figure 4). It is also notable that the relative populations of the two states in the first tier (D',δ) change as well (see Figures 4 and 5). Also in this case the lower energy component at (15 900 cm^{-1}) increases relatively compared to the higher energy component (17 300 cm^{-1}) in the visible region. At the same time, the emission from the spin-orbit excited states relatively increases. Note that already at 2% Xe doping the spin-orbit transitions are clearly observable (see Figure 5). Interestingly, very similar effect of increased D′-state population is observed at higher temperatures of pure I_2/Kr matrices.[5] This however might be a pure coincidence. This sequence can be understood by the following model: Interaction of the IP states with Xe atoms lead to increased solvation energy which leads to curve crossing with the repulsive spin-orbit excited states and non-radiative relaxation to them. The curve crossing occurs earlier for the first IP tier states that explains why emission from them decreases relatively. At the same time there is very little effect on the shape of the emission spectra upon complexation which seems to indicate that the change in solvation energy upon addition of one Xe atom is relatively small. We can estimate it assuming that addition of each Xe atom in the first solvation shell increases solvation energy linearly. The spectral shift for absorption is 2100 cm^{-1} for a Xe–I_2 complex when going from Kr to Xe environment. The number of nearest neighbors for I_2 in fcc lattice is 18 (Refs. 28 and 39), which leads to average solvation energy of ~120 cm^{-1} per added Xe atom. Taking into account the width of the bands and spectral overlap with the bands of monomeric iodine in the matrix, it is understandable that it would be difficult to observe the spectral shift for the complex if it radiates.

It is interesting to compare the situation with the gas-phase. Randall *et al.* observed in the gas-phase that the emission from the first IP tier D-state is very efficiently quenched in the presence of Kr with 193 nm excitation, and the observed emission originates from a "I_2–Kr cluster band" centered at ~423 nm.[41] This structure was previously attributed to the formation of I_2–Kr charge-transfer exciplex observed also in solid Kr.[23] When Xe is used for cluster formation instead of Kr, similar quenching of the D-state and population of the D′-state is observed for the low Xe pressures, but for the higher Xe pressures all of the first IP tier emissions are efficiently quenched implying enhancement of non-radiative decay channel similar to our Xe doped matrices. Partly this effect has been attributed in the gas-phase to the reactive quenching and formation of XeI* (emission at 253 nm) excimer by absorption of two 193 nm photons. Note that diatomic species like I*Xe are not typically observed in emission of solid rare gas samples with UV excitation, instead a

fast formation of triatomic exciplexes (I^-–Rg_2^+) is observed.[42] Reactive quenching of I_2 by Xe atoms in bulk conditions is also suggested as the reason for significant drops in the rates of collisionally induced nonadiabatic transitions between the second IP tier transitions (transitions from f to F) (Ref. 9). We however do not see any evidence of Xe-induced reactivity of I_2 in emission (dissociation) with the lowest Xe doping levels (<2%) in solid Kr. One can also question whether the Xe-induced non-radiative relaxation to the spin-orbit excited valence states is enough to explain the dramatic relative intensity losses from the first IP tier emissions. This possibility would require existence of another non-radiative channel, in addition to the relaxation to the spin-orbit states. This process would occur most likely through very efficient energy transfer within the I_2–Xe complex. The complex at least is clearly present in the lowest Xe doping levels in our samples. We acknowledge that efficient "totally dark" quenching of I_2 emissions in the I_2–Xe complex is a real possibility based on the strong emission intensity drops. However, only direct evidence of non-radiative relaxation we see in this work is the relaxation to the states in the I*-I* limit.

When higher Xe dopings are used dramatic changes are observed. Up to 17% doping, the emissions redshift in a normal way. The second IP tier emissions F → a′ and f → B show a respective redshifts of 500 cm^{-1} and ~400–500 cm^{-1} within the range of Xe ratios 0%–17%. At 50% doping, a new broad and blue-shifted emission belonging to a triatomic charge-transfer species between iodine atoms and Xenon (I^-–Xe_2^+) has appeared.[43] Helbing and Chergui suggested that the blue-shifted band has also a contribution from an anomalously shifted first IP tier emission, originating from the δ-state, only observed with 193 nm excitation.[44] Our systematic doping shows that this is not the case. The first and the second tier IP emissions undergo a normal redshift in the higher Xe doping levels. In pure Xe with 193 nm excitation, we observe mainly two type of transitions: a continuum-type of emission (with a apparent peak-like maximum at 26 500 cm^{-1}) with weaker counter parts in the visible (maximum at ~19 000 cm^{-1} and ~22 000 cm^{-1}), and sharp valence spin-orbit transitions (15 500–14 000 cm^{-1} region). The emission from the I^-–Xe_2^+ exciplex is readily observed in I_2/Xe matrices with 270 nm excitation.[44] Similarly, irradiation of IH with 277 nm excitation in solid Xe leads to rapid photodissociation and three "atomic" I^-–Xe_2^+ charge-transfer emissions with maxima at ~388 nm (25 800 cm^{-1}, $4^2\Gamma \rightarrow 1^2\Gamma$), ~460 nm (21 800 cm^{-1}, $4^2\Gamma \rightarrow 2^2\Gamma$), and ~560 nm (17 900 cm^{-1}, $4^2\Gamma \rightarrow 3^2\Gamma$) (Ref. 43). These transitions are very similar to emissions observed in the I_2 doped Xe with 193 excitation (26 500 cm^{-1}, 22 000^{-1}, 19 000 cm^{-1}). Our irradiation studies with 548 nm fs pulses also imply that these "atomic" species are photogenerated by I_2 dissociation in the matrix with 193 excitation (see supplementary material S1 for details[29]). Interesting notion is that the maxima of the emissions with 193 nm excitation and with fs 548 nm excitation are somewhat distinct from each other, as already argued in Ref. 44. Most pronounced spectral difference in solid Xe with the two wavelenghts is the lack of the most blue-shifted feature (peak-like maxima at 26 500 cm^{-1}) with the 548 nm excitation. Appearance of this feature with 193 nm excitation when the temperature is lowered,[44] or as in our case Xe ratio is increased from 50% to 100%, suggests a possible site effect. In any case, transitions observed in the solid Xe are *not* from the first IP tier transitions of I_2.

The conclusions drawn for the low level doping are valid also for high level doping. Increasing the amount of Xe in the matrix brings down energetically the IP states due to solvation leading to crossing with neutral repulsive states correlating with spin-orbit excited iodine atoms. This leads to non-radiative relaxation to the spin-orbit excited states. These effects are clearly seen in our data. The intensity of the emissions from the first IP tier states decreases first and this effect can be seen in the evolution of the main emission band (Figure 6). The depopulation of the first IP tier states can be seen in the disappearance of the red emissions. Simultaneously, the emissions from the spin-orbit excited states appear and gain intensity. Note that for example at 17% Xe doping the emission from the second IP tier is well visible although the red emission of the first IP tier have disappeared.

To summarize the emission results, we observe strong relative drops from the first IP tier emissions in favor of the second IP tier emissions upon doping I_2/Kr matrices with Xe, implying non-radiative relaxation of the first IP tier population to the doubly spin-excited states. With small Xe doping relaxed emission from the IP states does not show any indication of new emissions. Plausible reason for this is that complexation of I_2 with Xe either induces very efficient non-radiative relaxation or the emission from the complex cannot be separated from the uncomplexed iodine. With higher Xe doping levels IP emissions redshift in a normal way due to increased solvation, leading ultimately to a very efficient population of the spin-excited states. With higher Xe dopings or in pure Xe the I_2 molecule efficiently photodissociates with 193 excitation producing emission from I^-–Xe_2^+ species.

C. Pump-probe

The pump-probe experiment reveals small spectral changes induced by Xe atom which are very difficult to observe in 193 nm induced emission spectra. The contour plot in Figure 7 shows that the experiment can be used to separate emissions from the second and the first IP tiers (see Figure 1(c)). The cuts at −3 ps and +3 ps, presented in the lower panels (a) and (b) show slight spectral broadening effects induced by Xe for emissions originating from the first IP tier (−3 ps). For the emission from the second IP tier broadening is not evident (+3 ps). There is an increase in the sideband at 400 nm in the panel (b) but this may be due to emission from the first IP tier states. Time-domain pump-probe dynamics of the I_2 A($^3\Pi_{1u}$)-state has been analyzed with great detail in the rare gas matrices,[4,45–47] mainly from the point of view of cage recombination and predissociation to the A′ state. The negative time signal in the panel (c) reflects slow Kr cage dynamics[25,48] (period ~630 fs) seen through the first IP tier emissions. We propose a multiphoton (1 × 620 nm + 2 × 558 nm) excitation route through the cage bound A-state (see Figure 1 panel (c)) as the main source for our signal in the negative time delays. This argument is based on our

power dependence analysis of the emissions (see supplementary material S4 for details[29]). At zero time delay (t = 0 ps), the emission spectrum is identical with the negative time delay spectra, implying that the absorbing first IP tier state is directly accessible from the I_2 ground state configuration by a multiphoton excitation. The signal on the positive delays shows also the characteristic Kr cage modulation in the time-domain signal, but this time seen through the higher energy second IP tier emissions. The weaker signal on the positive delays is mainly generated by multiphoton excitation, where the roles of the pulses have been reversed (2 × 558 nm + 1 × 620 nm). On the positive delays the excitation occurs most likely through repulsive doubly spin-exited states of I_2 (I*-I*). This was also the proposed mechanism in a similar experiment by Bihary *et al.* in solid argon.[25] We investigated the Xe doped matrix also with pulse energies: λ_{Pump} = 558 nm and λ_{Probe} = 500 nm. Using these energies strong first IP tier emissions can be observed with a definite B-state oscillation period up to 5 ps (see supplementary material S3 for details[29]). We compared our time-domain oscillation periods from the Xe doped matrix with the pure I_2/Kr data in Ref. 15, but we could not observe any notable differences between them.

The pump-probe experiments were designed to show a possible effect of a single Xe atom on the slow cage dynamics or the bound vibrational dynamics of I_2. However, by comparison of the signals from undoped (Xe = 0%) and doped matrices (Xe = 0.1%) it is evident there is *no* clear difference between them. Actually, the time traces and the energy spectra in all tried cases are strikingly similar and all observed signals can be attributed to the pure I_2 in solid Kr. This result is somewhat surprising because based on the absorption and simultaneous CARS measurements we know that I_2–Xe complex is present in our Xe doped samples. Thus the conclusion from the pump-probe experiments is that the 1:1 Xe–I_2 complex does not show any time specific signal. This results suggests that either I_2–Xe-complex *does not radiate* (at least not in the studied UV-visible region) or the pertubation in the relaxed emission to the pure I_2 in solid Kr is small enough that we *lack selectivity* to see the complex. Since the main interest here is the 1:1 complex we did not attempt to expand the experiments towards higher Xe dopings.

As a summary of the pump-probe results, we postulate that the possible reasons for the negative finding are: (i) Enhanced nonradiative relaxation in the complex that leads to escape of the complex from pump-probe detection that relies on detection of relaxed luminescence, or (ii) Solvation energy induced by one Xe atom is small enough that the presence of complexed I_2 cannot be separated from the relaxed IP emission of the uncomplexed I_2.

V. CONCLUSIONS

Interaction of Xe with I_2 in a krypton matrix has been studied by electronic spectroscopy and pump-probe experiments. The goal of the study was to investigate electronic states and dynamics of 1:1 Xe–I_2 complex in solid Kr. In absorption the complex shows a specific signal redshifted by 2400 cm^{-1} from the absorption of uncomplexed I_2. The redshift can be interpreted to originate from Xe induced symmetry breaking, formation of a polar ion-pair state of I_2, and its electrostatic solvation in a polarizable Kr host. Possibility of charge-transfer absorption between Xe and I_2 cannot however be ruled out. When more Xe is added to the sample the absorption shifts further to red finally reaching its position in pure Xe host with a total shift of 5700 cm^{-1} from the gas-phase, indicating that in a Xe matrix the absorbing state is symmetry broken polar state. In emission there is no clear signal that could be assigned to the 1:1 Xe–I_2 complex but small shifts and broadening of the I_2 emissions is observed. Instead, it is found that complexation induces non-radiative relaxation to the spin-excited states of I_2. This is interpreted to originate from Xe induced increase in electrostatic solvation energy of the ion-pair states which leads to curve crossing of the first tier ion-pair states with the spin-excited valence states. Consistent with this, emissions from the second ion-pair tier gain intensity relative to the emissions from the first ion-pair tier. Emission from the ion-pair states was used as an observable in these experiments. In both cases the observed dynamics was characteristic of matrix-isolated I_2 and no clear signals specific to the I_2–Xe complex were observed. Possible reason for this is that the complex relaxes non-radiatively.

ACKNOWLEDGMENTS

This work was financially supported by Academy of Finland (Decision Number 122620) and Emil Aaltonen foundation.

[1] R. S. Mulliken, J. Chem. Phys. **55**, 288 (1971).
[2] J. C.D. Brand and A. R. Hoy, Appl. Spectrosc. Rev. **23**, 285 (1987).
[3] V. S. Batista and D. F. Coker, J. Chem. Phys. **105**, 4033 (1996).
[4] V. S. Batista and D. F. Coker, J. Chem. Phys. **106**, 6923 (1997).
[5] J. Helbing and M. Chergui, J. Chem. Phys. **115**, 6158 (2001).
[6] T. Kiviniemi, J. Aumanen, P. Myllyperkiö, V. A. Apkarian, and M. Petterson, J. Chem. Phys. **123**, 064509 (2005).
[7] A. Scaria, V. Namboodiri, J. Konradi, and A. Materny, Phys. Chem. Chem. Phys. **10**, 983 (2008).
[8] A. L. Guy, K. Viswanathan, A. Sur, and J. Tellinghuisen, Chem. Phys. Lett. **73**, 582 (1980).
[9] M. E. Akopyan, I. Y. Novikova, S. A. Poretsky, A. M. Pravilov, A. G. Smolin, T. V. Tscherbul, and A. A. Buchachenko, J. Chem. Phys. **122**, 204318 (2005).
[10] N. Yu and D. F. Coker, Mol. Phys. **102**, 1031 (2004).
[11] V. A. Apkarian and N. Schwentner, Chem. Rev. **99**, 1481 (1999).
[12] R. Zadoyan, M. Sterling, and V. A. Apkarian, J. Chem. Soc., Faraday Trans. **92**, 1821 (1996).
[13] C. Lienau and A. H. Zewail, J. Phys. Chem. **100**, 18629 (1996).
[14] A. Materny, C. Lienau, and A. H. Zewail, J. Phys. Chem. **100**, 18650 (1996).
[15] M. Bargheer, M. Gühr, P. Dietrich, and N. Schwentner, Phys. Chem. Chem. Phys. **4**, 75 (2002).
[16] Y. Nakano, H. Fujiwara, M. Fukushima, and T. Ishiwata, J. Chem. Phys. **128**, 164320 (2008).
[17] G. Handcock, G. Richmond, G. A.D. Ritchie, and S. Taylor, Phys. Chem. Chem. Phys. **11**, 6415 (2009).
[18] M. E. Akopyan, I. Y. Novikova, S. A. Poretsky, A. M. Pravilov, A. G. Smolin, T. V. Tscherbul, and A. A. Buchachenko, J. Chem. Phys. **130**, 124302 (2009).
[19] M. E. Akopyan, S. S. Lukashov, S. A. Poretsky, A. M. Pravilov, A. S. Torgashkova, A. A. Buchachenko, and Y. V. Suleimanov, J. Chem. Phys. **129**, 114309 (2009).
[20] J. Liebers, A. Scaria, A. Materny, and U. Kleinekathöfer, J. Raman Spectrosc. **40**, 822 (2009).
[21] J. Liebers, A. Scaria, A. Materny, and U. Kleinekathöfer, Phys. Chem. Chem. Phys. **12**, 1351 (2010).

[22]T. Kiviniemi, E. Hulkko, and M. Pettersson, Chem. Phys. Lett. **491**, 44 (2010).
[23]M. Macler and M. C. Heaven, Chem. Phys. **151**, 219 (1991).
[24]M. Gühr, P. Dietrich, and N. Schwentner, J. Phys. Chem. A **106**, 12002 (2002).
[25]Z. Bihary, R. Zadoyan, M. Karavitis, and V. A. Apkarian, J. Chem. Phys. **120**, 7576 (2004).
[26]J. Almy, K. Kizer, R. Zadoyan and V. A. Apkarian, J. Phys. Chem. A **104**, 3508 (2000).
[27]M. Karavitis, T. Kumada, I. U. Goldschleger, and V. A. Apkarian, Phys. Chem. Chem. Phys. **7**, 791 (2005).
[28]T. Kiviniemi, T. Kiljunen, and M. Petterson, J. Chem. Phys. **125**, 164302 (2006).
[29]See supplementary material at http://dx.doi.org/10.1063/1.4706521 for (S1) Irradiation of Xe = 100% matrix with 548 nm excitation, (S2) Fs-CARS measurements of matrices with Xe = 0% and Xe = 0.1%, (S3) Pump-probe dynamics of Xe = 0.1% with λ_{Pump} = 558 nm and λ_{Probe} = 500 nm, and (S4) Power dependence analysis of the pump-probe emissions with λ_{Pump} = 558 nm and λ_{Probe} = 620 nm.
[30]L. M. Julien and W. B. Parson, J. Chem. Phys. **72**, 3059 (1968).
[31]H. A. Benesi and J. H. Hildebrand, J. Am. Chem. Soc. **71**, 2703 (1949).
[32]R. S. Mulliken, J. Am. Chem. Soc. **72**, 600 (1950).
[33]T. Kiviniemi, E. Hulkko, T. Kiljunen, and M. Pettersson, J. Phys. Chem. A **112**, 5025 (2008).
[34]T. Kiviniemi, E. Hulkko, T. Kiljunen, and M. Pettersson, J. Phys. Chem. A **113**, 6326 (2009).
[35]F. Brandi, I. Velchev, W. Hogervorst, and W. Ubachs, Phys. Rev. A **64**, 032505 (2001).
[36]W. Person, J. Chem. Phys. **38**, 109 (1963).
[37]L. Onsager, J. Am. Chem. Soc. **58**, 1486 (1936).
[38]R. L. Amey and R. H. Cole, J. Chem. Phys. **40**, 146 (1964).
[39]M. Karavitis and V. A. Apkarian, J. Phys. Chem. B **106**, 8466 (2002).
[40]R. J. Donovan, M. A. MacDonald, K. P. Lawley, and A. J. Yencha, Chem. Phys. Lett. **138**, 571 (1987).
[41]K. L. Randall and D. J. Donaldson, Chem. Phys. **211**, 377 (1996).
[42]M. E. Fajardo and V. A. Apkarian, J. Chem. Phys. **89**, 4102 (1988).
[43]W. Lawrence, F. Okada, and V. A. Apkarian, Chem. Phys. Lett. **150**, 339 (1988).
[44]J. Helbing and M. Chergui, J. Lumin. **94**, 611 (2001).
[45]R. Zadoyan, Z. Li, C. C. Martens, and V. A. Apkarian, J. Chem. Phys. **101**, 6648 (1994).
[46]Z. Li, R. Zadoyan, V. A. Apkarian, and C. C. Martens, J. Phys. Chem. **99**, 7453 (1995).
[47]R. Zadoyan, J. Almy, and V. A. Apkarian, Faraday Discuss. **108**, 255 (1997).
[48]M. Gühr, M. Bargheer, M. Fushitani, T. Kiljunen, and N. Schwentner, Phys. Chem. Chem. Phys. **9**, 779 (2007).